SIAM J. Sci. Comput.
Vol. 21, No. 1, pp. 294–322

HIGH-ORDER CENTRAL SCHEMES FOR HYPERBOLIC SYSTEMS OF CONSERVATION LAWS[*]

FRANCA BIANCO[†], GABRIELLA PUPPO[†], AND GIOVANNI RUSSO[‡]

Abstract. A family of shock capturing schemes for the approximate solution of hyperbolic systems of conservation laws is presented. The schemes are based on a modified ENO reconstruction of pointwise values from cell averages and on approximate computation of the flux on cell boundaries. The use of a staggered grid avoids the need of a Riemann solver. The integral of the fluxes is computed by Simpson's rule. The approximation of the flux on the quadrature nodes is obtained by Runge–Kutta schemes with the aid of natural continuous extension (NCE). This choice gives great flexibility at low computational cost. Several tests are performed on the scalar equation and on systems. The numerical results confirm the expected accuracy and the high resolution properties of the schemes.

Key words. conservation laws, central schemes, high order, Runge–Kutta

AMS subject classifications. 65M10, 65M05

PII. S1064827597324998

1. Introduction.

In this paper we present third- and fourth-order central schemes for the approximate solution of quasilinear systems of conservation laws. The schemes can be viewed as an extension of the second-order Nessyahu–Tadmor (NT) scheme [11]. The main advantage of central schemes over upwind schemes is that they do not require the solution of Riemann problems or the computation of characteristic velocities of the system [11, 14].

These features make the central scheme approach very attractive for those systems for which the solution to the Riemann problem is complicated or when there is no simple analytical expression for the eigenvalues of the Jacobian matrix.

This is the case of systems arising, for example, in semiconductor modeling [1, 13]. In that case the NT scheme, suitably modified to incorporate source terms, has been successfully used.

A third-order scheme has been presented by Liu and Tadmor [10]. They show that the scheme is *number of extrema decreasing* (NED), and it gives good numerical results both on the scalar equation and on the Euler equations.

The main focus of this paper is the development of third- and fourth-order schemes, which are robust and efficient, so that they can be easily implemented for several systems of conservation laws. The user has to provide only a subroutine for the computation of the flux vector and an estimate of the eigenvalues (necessary to satisfy the stability condition). This goal is obtained by using Runge–Kutta schemes with NCE for the integration of the flux.

The plan of the paper is the following. In section 2 we derive the schemes. Essentially nonoscillatory (ENO) and modified ENO reconstruction are presented. Two approaches for the computation of the flux are considered: Taylor expansion and Runge–Kutta schemes. We describe the use of Runge–Kutta with NCE for the in-

[*] Received by the editors July 21, 1997; accepted for publication (in revised form) June 10, 1998; published electronically September 1, 1999.

http://www.siam.org/journals/sisc/21-1/32499.html

[†] Dipartimento di Matematica, Politecnico di Torino, Corso Duca degli Abruzzi, Torino (puppo@polito.it). The research of this author was partially supported by MURST 40% Analisi Numerica.

[‡] Dipartimento di Matematica, Università dell'Aquila Via Vetoio, loc. Coppito - 67100 L'Aquila (russo@univaq.it).

tegration of the flux. Several schemes are derived, both of third and fourth order. In this fashion high-order black box schemes for systems of conservation laws are obtained. In section 3 we study the properties of the schemes. These include linear stability analysis of all schemes considered and the evaluation of the truncation error. The fourth section is devoted to numerical results. We consider the same tests described by Liu and Tadmor [10]. We start from the scalar equation, where the order of accuracy is computed on several smooth solutions, and we end with the shock tube problem of gas dynamics with different initial and boundary conditions.

2. Description of the method. In this section we describe our high-order central scheme. We start with a brief outline of the scheme for scalar equations in section 2.1 followed by a more detailed description of the several steps composing the method in the next subsections. Finally in section 2.5 the extension of the scheme to systems of conservation laws is considered.

2.1. Central schemes for scalar conservation laws. We want to solve the scalar conservation law

$$u_t + f_x(u) = 0, \tag{2.1}$$

on an interval I, with suitable boundary conditions. We consider for simplicity a uniform grid on I of points $\{x_j\}$, $j = 0, \dots, N$, with $x_{j+1} - x_j = h$. Let k be the time step, with $u_j^n = u(x_j, t^n)$, $t^n = nk$. Finally w will denote the computed solution of (2.1).

At time t^n, we start from a piecewise constant function $\overline{w}_j^n$, representing the cell averages of the computed solution w at time t^n, namely,

$$\overline{w}_j^n = \frac{1}{h}\int_{-h/2}^{h/2} w(x_j + y, t^n)\, dy. \tag{2.2}$$

From the values $\{\overline{w}_j^n\}_{j=0}^N$ we reconstruct the point values of the function $w(x, t^n)$ via a suitable nonlinear piecewise polynomial interpolation. The reconstruction we use is due to Harten, Engquist, Osher, and Chakravarthy [3]. We will describe our implementation of the reconstruction step in section 2.2 for completeness. Let $\mathcal{R}(\overline{w}^n;\ x)$ be the reconstruction operator, where $\overline{w}^n$ is the vector with components $\overline{w}_j^n$, $j = 0, \dots, N$. Then

$$w(x, t^n) := \mathcal{R}(\overline{w}^n;\ x) \tag{2.3}$$

is the function defined on I which will be used as initial data for the nth time step. The reconstruction $\mathcal{R}(\overline{w}^n;\ x)$ is piecewise polynomial in the sense that

$$\mathcal{R}(\overline{w}^n;\ x) \in P_j^m \qquad \text{for } x \in \left[x_j - \frac{h}{2}, x_j + \frac{h}{2}\right],$$

where P_j^m is the space of polynomials of degree m defined on the interval $[x_j - h/2, x_j + h/2]$. Note that in general $\mathcal{R}$ will have jump discontinuities at the points $x_j \pm h/2$.

The evolution of the discontinuous data $w(x, t^n)$ can be computed by solving a sequence of generalized Riemann problems centered at the points $x_{j+1/2} = x_j + h/2$. If the time step is restricted by the CFL condition as $k \le h/\max|f'(u)|$, then the Riemann problems remain decoupled. This is the framework of upwind methods (see [6] and references therein), where the updated solution is given by

$$\overline{w}_j^{n+1} = \overline{w}_j^n - \lambda\frac{1}{k}\int_0^k \left[f\left(w(x_{j+1/2}, t^n + \tau)\right) - f\left(w(x_{j-1/2}, t^n + \tau)\right)\right] d\tau, \tag{2.4}$$

where $\lambda = k/h$. The computation of $w(x_{j+1/2}, t^n + \tau)$ requires the (approximate) solution of the generalized Riemann problem at $x_{j+1/2}$. In the case of systems of conservation laws, this step is the most expensive building block of upwind schemes.

On the other hand, in central schemes, the solution is updated on a staggered grid. Thus, following Liu and Tadmor, [10], and Nessyahu and Tadmore, [11], we compute

$$\begin{aligned} \overline{w}^{n+1}_{j+1/2} &= \frac{1}{h}\left\{\int_0^{h/2} w(x_j + y, t^n)\, dy + \int_{-h/2}^{0} w(x_{j+1} + y, t^n)\, dy\right\} \\ &\quad -\lambda \frac{1}{k}\int_0^k \left[f\left(w(x_{j+1}, t^n + \tau)\right) - f\left(w(x_j, t^n + \tau)\right)\right] d\tau; \end{aligned} \tag{2.5}$$

i.e., we integrate the conservation law on the staggered cells $[x_j, x_{j+1}] \times [t^n, t^n + k]$. If the time step is subjected to the more restrictive CFL condition $k \le h/(2 \max |f'(u)|)$, we can assume that $w(x, t^n + \tau)$ is smooth at x_{j+1} and x_j, since the discontinuities starting at t^n from the staggered grid points $x_{j+1/2}$ have not had the time to reach the cell boundaries.

Then the time integrals can be evaluated with a quadrature formula, say,

$$\frac{1}{k}\int_0^k f\left(w(x_j, t^n + \tau)\right)\, d\tau \simeq \sum_{l=0}^{L} f\left(w(x_j, t^n + k\tau_l)\right)\omega_l, \tag{2.6}$$

where τ_l and $\omega_l \in [0, 1]$ are the knots and weights of the quadrature formula.

Since w is smooth at x_j, we can evaluate w at the intermediate times $t^n + k\tau_l$ through Taylor expansion (see section 2.3) or with a Runge–Kutta method (see section 2.4).

In the following time step we repeat a similar process and go back to the original grid.

Thus, in Godunov type upwind methods the weak form of the conservation law is enforced in cells in space–time which are arranged like a pile of boxes. In central type schemes, the weak form of the conservation law is enforced on cells which are arranged like bricks in a wall (with due care to boundary conditions), as is shown in Figure 2.1.

Upwind schemes enjoy a less restrictive CFL condition and are characterized by a smaller amount of artificial diffusion. The main advantage of central schemes is their simplicity: each time step is faster and their implementation is easier. See [4], [9], and [14] for a discussion of the advantages of central schemes in a multidimensional setting.

2.2. Reconstruction. Reconstruction is a key step in high resolution schemes. The algorithm we consider here was introduced in [3] and it has been widely implemented; see [16] and references therein. In this section we review the basic facts which are essential for the construction of our scheme.

We will need two kinds of reconstruction:

(a) Given the point values of a function $w(x_j)$, we build a piecewise polynomial interpolant $\mathcal{I}$ to evaluate the x-derivatives of w at the grid points x_j's (piecewise polynomial interpolation, see section 2.2.1).

(b) Given the cell averages $\overline{w}_j$ of a function w, we reconstruct the point values $w(x)$ and the x-derivatives of w at the grid points x_j's (reconstruction via deconvolution; see section 2.2.2).

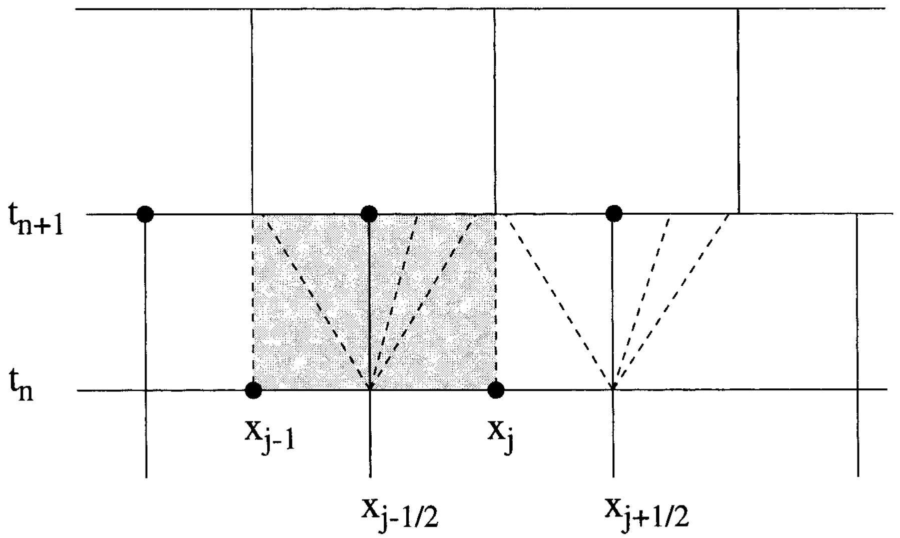

FIG. 2.1. *NT scheme on a staggered grid.*

2.2.1. ENO piecewise polynomial interpolation. Given the point values $\{(x_j, w_j)\}_{j=0}^{N}$ of a function $w(x)$, we find an interpolant $\mathcal{I}_w^r(x)$ of degree r such that

1. $\mathcal{I}_w^r(x_j) = w_j$;
2. $\mathcal{I}_w^r(x) \in P_j^r$ for $x \in [x_j - h/2, x_j + h/2]$;
3. If u is a smooth function, $\mathcal{I}_u^r(x) - u(x) = e(x)h^{r+1} + O(h^{r+2})$, where $e(x)$ is at least piecewise continuous;
4. $\mathcal{I}_w^r$ is ENO in the sense of Harten et al. in [3].

We start from the construction of a local polynomial $\tilde{q}_{j+1/2}^r(x)$ of degree r, defined on $[x_j, x_{j+1}]$, satisfying the interpolation conditions

$$\tilde{q}_{j+1/2}^r(x_j) = w_j \qquad \text{and} \qquad \tilde{q}_{j+1/2}^r(x_{j+1}) = w_{j+1}. \tag{2.7}$$

To satisfy the accuracy condition 3, we further require

$$\tilde{q}_{j+1/2}^r(x_l) = w_l \qquad \text{for } l \in \{il(j), \ldots, il(j) + r\}, \tag{2.8}$$

where $x_{il(j)}$ is the leftmost point of the stencil on which the construction of $\tilde{q}_{j+1/2}^r(x)$ is based. The interpolation condition (2.7) requires that $j - r + 1 \le il(j) \le j$. Thus the conditions (2.7) and (2.8) are satisfied by r polynomials. We use this freedom to select the polynomial that is less oscillatory. The problem of the best choice of $il(j)$ is still not settled; see [3], [12], [15] and subsection 2.2.3 below.

Once $il(j)$ has been chosen for all j, we construct the polynomial $\tilde{q}_{j+1/2}^r(x)$ from the coefficients of the table of divided differences based on the points $(x_{il(j)}, w_{il(j)}), \ldots, (x_{il(j)+r}, w_{il(j)+r})$.

Gluing together the $\tilde{q}_{j+1/2}^r$'s, we obtain a continuous interpolant with jumps in the first and higher derivatives at the grid points x_j's. We now observe that if $\tilde{q}$

interpolates the point values of a smooth function u, then

$$\begin{aligned} H_j^{+,l} &:= h^l \frac{d^l}{dx^l}\tilde{q}_{j+1/2}^r\Big|_{x_j+0^+} = h^l \frac{d^l}{dx^l}u\Big|_{x_j} + O(h^{r+1}), \\ H_j^{-,l} &:= h^l \frac{d^l}{dx^l}\tilde{q}_{j-1/2}^r\Big|_{x_j+0^-} = h^l \frac{d^l}{dx^l}u\Big|_{x_j} + O(h^{r+1}). \end{aligned} \tag{2.9}$$

Now let

$$D_j^l = \mathrm{MinMod}(H_j^{+,l}, H_j^{-,l}), \tag{2.10}$$

where MinMod is as usual:

$$\mathrm{MinMod}(x,y) = \begin{cases} s\min(|x|,|y|) & \text{if } \mathrm{sgn}(x) = \mathrm{sgn}(y) = s, \\ 0 & \text{otherwise.} \end{cases}$$

We finally define

$$q_j^r(x) = \sum_{l=0}^{r} \frac{1}{l!} D_j^l \left(\frac{x-x_j}{h}\right)^l, \qquad x \in \left[x_j - \frac{h}{2}, x_j + \frac{h}{2}\right], \tag{2.11}$$

and

$$w(x) = \mathcal{I}_w^r(x),$$

where

$$\mathcal{I}_w^r(x) = q_j^r(x) \qquad \text{for} \qquad x \in \left[x_j - \frac{h}{2}, x_j + \frac{h}{2}\right]. \tag{2.12}$$

Thus, if u is a smooth function, then

$$h^l\left(\frac{d^l u(x)}{dx^l} - \frac{d^l \mathcal{I}_u^r(x)}{dx^l}\right) = O(h^{r+1}), \qquad 0 \le l \le h, \tag{2.13}$$

except at the points $x_{j+1/2}$, where $\mathcal{I}_u^r$ will be discontinuous in general. Note, however, that the accuracy may deteriorate locally due to the clipping phenomena introduced with the MinMod function on local extrema.

2.2.2. Reconstruction via deconvolution. Suppose we are given the cell averages $\{\overline{u}_j\}$ of a smooth function $u(x)$. We consider the cell averaged function:

$$\overline{u}(x) = \frac{1}{h}\int_{-h/2}^{h/2} u(x+y)\, dy.$$

We construct the piecewise polynomial interpolant of $\overline{u}(x)$ described in the previous subsection, namely, $\mathcal{I}_{\overline{u}}^r(x)$. Expanding the integrand appearing in the definition of $\overline{u}$, we find

$$\overline{u}(x) = \frac{1}{h}\sum_{l=0}^{\infty}\frac{1}{l!}\frac{d^l u}{dx^l}\Big|_x \int_{-h/2}^{h/2} y^l\, dy = \sum_{l=0}^{\infty} h^l \alpha_l \frac{d^l u}{dx^l}\Big|_x, \tag{2.14}$$

where

$$\alpha_l = \frac{1}{h}\frac{1}{l!}\frac{1}{h^l}\int_{-h/2}^{h/2} y^l\, dy = \begin{cases} \dfrac{1}{(l+1)!}\left(\dfrac{1}{2}\right)^l & l \text{ even,} \\ 0 & l \text{ odd.} \end{cases}$$

Moreover,

$$\frac{d^k\overline{u}(x)}{dx^k} = \sum_{l=0}^{\infty} h^l \alpha_l \left.\frac{d^{l+k}u}{dx^{l+k}}\right|_x .$$

Thus,

$$h^k \frac{d^k\overline{u}(x)}{dx^k} = \sum_{l=0}^{r-k} h^{k+l}\alpha_l \left.\frac{d^{l+k}u}{dx^{l+k}}\right|_x + O(h^{r+1}), \qquad k = 0, \dots, r. \tag{2.15}$$

We now let $x = x_j$, and we approximate the left-hand side with the interpolant $\mathcal{I}^r_{\overline{u}}$:

$$D^k_j = \sum_{l=0}^{r-k} h^{k+l}\alpha_l \left.\frac{d^{l+k}u}{dx^{l+k}}\right|_{x_j} + O(h^{r+1}), \qquad k = 0, \dots, r, \tag{2.16}$$

where the D^k_j's have been defined in (2.10). Next we define the quantities $\tilde{D}^l_j$ through the linear system:

$$D^k_j = \sum_{l=0}^{r-k} \alpha_l \tilde{D}^{l+k}_j, \qquad k = 0, \dots, r. \tag{2.17}$$

Clearly

$$\tilde{D}^l_j = h^l \left.\frac{d^l u}{dx^l}\right|_{x_j} + O(h^{r+1}), \qquad l = 0, \dots, r,$$

and the reconstruction is given by

$$\mathcal{R}(\overline{u}^n;\ x) = \sum_{l=0}^{r} \frac{1}{l!}\tilde{D}^l_j \left(\frac{x - x_j}{h}\right)^l, \qquad x \in \left[x_j - \frac{h}{2}, x_j + \frac{h}{2}\right]. \tag{2.18}$$

Note that the system for the $\tilde{D}^l_j$'s is upper triangular and can be solved via back substitution. By construction we have that $1/h \int_{-h/2}^{h/2} \mathcal{R}(\overline{u}^n;\ x_j + y)\, dy = \overline{u}_j$, so that conservation is exactly enforced. This means that in general $\mathcal{R}(\overline{u}^n;\ x_j) \neq u_j$.

2.2.3. Choosing the stencil. We still need to specify a recipe for choosing the stencil of the polynomials $\tilde{q}^r_{j+1/2}$ defined in section 2.2.1.

The divided differences appearing in the coefficients of $\tilde{q}^r_{j+1/2}$ are computed from the data $(x_{il(j)}, w_{il(j)}) \cdots (x_{il(j)+r}, w_{il(j)+r})$. If the function $w(x)$ is smooth in the interval $(x_{il(j)}, x_{il(j)+r})$, then the polynomial $\tilde{q}^r_{j+1/2}$ will have no spurious oscillations.

On the other hand, if $w(x)$ or its derivatives of order $l \leq r$ have jumps in the interval $(x_{il(j)}, x_{il(j)+r})$, then $\tilde{q}^r_{j+1/2}$ will exhibit an oscillatory Gibbs phenomenon.

Thus we need to choose $il(j)$ so that the interval $(x_{il(j)}, x_{il(j)+r})$ lies in a region of smoothness of w. This requires that the exact solution does not have points of discontinuity that are too close. In particular, when two shocks interact, the scheme might develop some local oscillations, until the waves separate.

The Harten–Engquist–Osher–Chakravarthy (HEOC) stencil. The algorithm proposed by Harten et al. in [3] is

```
(2.19)
$il(j) = j$
for $l = 2, \dots, r$
        if $\left|w[x_{il(j)}, \dots, x_{il(j)+l}]\right| > \left|w[x_{il(j)-1}, \dots, x_{il(j)+l-1}]\right|$
            $il(j) := il(j) - 1$
end for
```

where $w[x_{il(j)}, \dots, x_{il(j)+l}]$ is the divided difference of order l based on the abscissas $x_{il(j)}, \dots, x_{il(j)+l}$. Thus, we select the stencil yielding the smallest divided differences. For more details, see [3].

With this technique, the position of the stencil is very sensitive to small variations in the data $\{w_j\}$. Thus, in some cases the behavior of $il(j)$ versus j can be very irregular. This phenomenon does not lead to oscillations in the computed solution, but it can result in a severe loss of accuracy. See [12] and [15] for a discussion of this problem for upwind schemes and our numerical results in section 4 for a central scheme setting.

Shu's stencil. This algorithm for choosing $il(j)$ was proposed in [15] and it is designed to regularize the behavior of $il(j)$ versus j.

The idea is that the loss of accuracy experienced with the HEOC stencil may be due to the fact that the scheme can temporarily select linearly unstable stencils. Let $jc(j)$ be the position of the stencil which is locally linearly stable. Then Shu biases the choice of $il(j)$ toward $jc(j)$. Namely,

```
(2.20)
    $il(j) = j$
    for $l = 2, \dots, r$
        if $il(j) > jc(j)$ then
            if $\omega \left| w[x_{il(j)}, \dots, x_{il(j)+l}] \right| > \left| w[x_{il(j)-1}, \dots, x_{il(j)+l-1}] \right|$
                $il(j) := il(j) - 1$
        if $il(j) \leq jc(j)$ then
            if $\left| w[x_{il(j)}, \dots, x_{il(j)+l}] \right| > \omega \left| w[x_{il(j)-1}, \dots, x_{il(j)+l-1}] \right|$
                $il(j) := il(j) - 1$
    end for
```

where ω is a weight. Shu proposes $\omega = 2$.

In our central scheme setting, we cannot compute $jc(j)$ starting from the wind direction, otherwise we would have to compute the sign of characteristic velocities, and this would destroy the simplicity of the scheme. Thus, we set $jc(j) =$ central stencil. With this simplification, the performance of Shu's stencil deteriorates; see section 4.

The MC stencil. Our numerical experiments give the best results with the *MC* (mostly centered) stencil which we propose. The central stencil can be defined as

$$il(j) := j - [r/2],$$

where r is the degree of the polynomial used in the reconstruction, $\mathcal{R}(\overline{w}^n;\ x)$, and $[x]$ is the integer part of x. The idea is to choose the central stencil when the function w_j is monotone and to fall back on the HEOC stencil if an oscillation in the data $\{w_j\}$ is detected.

The advantage of this simple procedure is twofold: the behavior of $il(j)$ versus j becomes very stable, and this has a favorable effect on the truncation error (see section 3.2). Moreover, linear stability analysis shows that the central stencil is linearly stable for all our schemes. This, according to our computations and the results shown in [12] and [15], seems to be crucial for high accuracy; see also section 4.

On the other hand, we are able to exploit the nonoscillatory properties of the HEOC stencil when the exact solution has a discontinuity; see section 4.1.

Moreover, if the exact solution has bounded derivatives, the central stencil minimizes the error due to polynomial interpolation.

2.3. Evaluation of the fluxes via Taylor expansion. To compute the time integrals of the fluxes in (2.6), we need to evaluate the function $f(w(x_j, t^n + k\tau_l))$ at the different instants $k\tau_l \in [0, k]$, $l = 0, \ldots, L$. From the reconstruction step, we have the values $w(x_j, t^n)$ and the derivatives $d^l w/dx^l(x_j, t^n)$, for $l = 1, \ldots, m$. Since w is smooth at x_j, we can expand $w(x, t^n + \tau)$ in a Taylor series:

$$w(x_j, t^n + \tau) = \sum_{\nu=0}^{r} \frac{1}{\nu!} \frac{\partial^\nu w}{\partial t^\nu}(x_j, t^n)\tau^\nu + O(h^{r+1}). \tag{2.21}$$

For a method of order m, it is enough to consider $r = m - 1$; see section 3.2.

To evaluate the t-derivatives of w, we use the conservation equation. This can be done in two ways.

A first possibility is to compute

$$w_t = -f_x(w).$$

With this approach, the computation of $w_t(x_j, t^n)$ at all grid points requires the following steps:

- Compute $f(w(x_j, t^n))$ $\forall j$.
- Perform an interpolation of the grid values of f, as in section 2.2.1.
- Compute the x-derivative of the interpolant at the grid points.

Similarly the higher order derivatives for the scalar equation are given by

$$\begin{aligned} w_{tt} &= -\partial_x \left(f' w_t\right), \\ w_{ttt} &= -\partial_x \left(f''(w_t)^2 + f' w_{tt}\right). \end{aligned} \tag{2.22}$$

With this approach, for a method of order $m = 4$ we need to compute only the first and the second derivative of f. On the other hand, each time derivative requires an interpolation step. This strategy will be called *Timed*.

A second possibility is to compute

$$w_t = -f'(w) w_x,$$

and similarly

$$\begin{aligned} w_{tt} &= 2f'f''(w_x)^2 + (f')^2 w_{xx}, \\ w_{ttt} &= -6(f'')^2 f'(w_x)^3 - 3(f')^2 f'''(w_x)^3 - 9(f')^2 f'' w_x w_{xx} - (f')^3 w_{xxx}. \end{aligned} \tag{2.23}$$

These formulas become clearly prohibitively complex when applied to systems of equations. However, this approach is very fast for scalar equations, because we need to perform only one interpolation per time step. This strategy will be called *Timeux* in section 4.

2.4. Evaluation of the fluxes through a Runge–Kutta method. The time integrals of the fluxes in (2.6) can also be evaluated with a Runge–Kutta method. In this fashion no computation of the derivatives of f is required.

We consider the conservation law at the grid points $x = x_j$. At each of these points, the PDE reduces to an autonomous ODE in the time variable t.

Consider the Cauchy problem

$$\begin{cases} y' = F(t, y(t)), \\ y(t_0) = y_0. \end{cases}$$

We adapt to our case the notation used in [19]. Then the solution at the $(n+1)$th time step obtained with a ν stage Runge–Kutta scheme can be written as

$$y^{n+1} = y^n + k \sum_{i=1}^{\nu} b_i g^{(i)},$$

where the $g^{(i)}$'s are the approximate Runge–Kutta fluxes,

$$g^{(i)} = F\biggl(t^n + kc_i, y^n + k \sum_{j=1}^{\nu-1} a_{i,j} g^{(j)}\biggr),$$

and the c_i are given by $c_i = \sum_j a_{i,j}$. The method is of course completely determined by the vector b and the matrix a, which is lower triangular for explicit schemes.

In our case, we are solving a sequence of Cauchy problems. At the jth grid point we have

$$\left\{ \begin{array}{rcl} y'(\tau) & = & F(\tau, y(\tau)) = -f_x\left(y(x_j, t^n + \tau)\right), \\ y(\tau = 0) & = & w(x_j, t^n). \end{array} \right. \tag{2.24}$$

Thus the computation of the ith Runge–Kutta flux $g^{(i)}$ requires the evaluation of the x-derivative of f at the intermediate time $t = t^n + c_i k$.

Therefore, we must compute all grid values of f at the intermediate time $t = t^n + c_i k$ and perform a piecewise polynomial interpolation of these data as in section 2.2.1 to maintain high accuracy and control over oscillations in the evaluation of f_x.

For a method of order $m = 4$, we need a third-order accurate three stage Runge–Kutta method. Thus we need to compute three polynomial interpolations for each node τ_l in the quadrature formula appearing in (2.6).

Fortunately a great saving in computational time can be obtained with the use of NCEs of a Runge–Kutta scheme. These will be reviewed in the next subsection.

2.4.1. NCEs. The properties of NCEs which are essential for their application to our scheme are described and proved in [19]. Here we state only the main facts.

Each ν-stage Runge–Kutta method of order p has a natural continuous extension u of degree $d \le p$ in the sense that there exist ν polynomials $b_i(\theta), i = 1, \dots, \nu$ of degree at most d such that

1. $u(t^n + \theta k) := y^n + k \sum_{i=1}^{\nu} b_i(\theta) g^{(i)}, \qquad 0 \le \theta \le 1;$
2. $u(t^n) = y^n$ and $u(t^n + k) = y^{n+1}$;
3. $\max_{t^n \le t \le t^n + k} \left| y^{(l)}(t) - u^{(l)}(t) \right| = O(h^{d+1-l}), 0 \le l \le d,$

where $y(t)$ is the exact solution of the equation with $y(t^n) = y^n$. Note that the polynomials $b_i(\theta)$ depend only on the Runge–Kutta method chosen and not on the particular ODE being solved.

Thus, at each time step, we apply the Runge–Kutta scheme only once, and we obtain all intermediate values $w(x_j, t^n + k\tau_l)$ through the evaluation of the appropriate NCE.

We end this section listing the NCEs which are of interest for our scheme.

$$
\begin{array}{ll}
(1) & RK1 \qquad \text{(for our second-order scheme)} \\
 & d=\nu=p=1, \\
 & b_1(\theta)=\theta; \\
(2) & RK2 \qquad \text{(for our third-order scheme)} \\
 & d=\nu=p=2, \\
 & b_1(\theta)=(b_1-1)\theta^2+\theta, \\
 & b_2(\theta)=b_2\theta^2; \\
(3) & RK3 \\
 & d=2,\nu=p=3, \\
 & b_i(\theta)=3(2c_i-1)b_i\theta^2+2(2-3c_i)b_i\theta, \qquad i=1,2,3, \\
 & \text{No NCE of degree } d=3 \text{ exists in this case;} \\
(4) & RK4 \qquad \text{(for our fourth-order scheme)} \\
 & d=3,\nu=p=4, \\
 & b_1(\theta)=2(1-4b_1)\theta^3+3(3b_1-1)\theta^2+\theta, \\
 & b_i(\theta)=4(3c_i-2)b_i\theta^3+3(3-4c_i)b_i\theta^2, \qquad i=2,3,4, \\
 & \text{No NCE of degree } d=4 \text{ exists in this case.}
\end{array}
\tag{2.25}
$$

Therefore, for $m=4$ we will compute the integral of the flux with a fourth-order RK scheme and its NCE of order three. This requires four function evaluations per time step. The alternative would be to use two RK3 steps, which requires six function evaluations.

2.5. Systems of conservation laws. We consider the system of conservation laws

$$\mathbf{u}_t+\mathbf{f}_x(\mathbf{u})=0, \tag{2.26}$$

where $\mathbf{u}$ and $\mathbf{f}$ are vectors with M components.

We apply our scheme componentwise. At each time step, we start from the array of cell averages, $\{\overline{w}^n_{j,i}\}, j=1,\dots,N;\ i=1,\dots,M$. We apply the reconstruction step, as described in section 2.2 at each component. The stencil chosen in general will be different for each component. The evaluation of the space contribution appearing in (2.5) is now straightforward.

The computation of the time integrals of the fluxes is a little more delicate.

If we approximate $\mathbf{w}(x_j,t^n+\tau)$ with its Taylor expansion as in (2.21), for the *Timed* method, we have

$$\mathbf{w}_t=-\partial_x\left(\mathbf{f}\right), \tag{2.27}$$

$$\mathbf{w}_{tt}=-\partial_x\left(J\mathbf{f}\cdot\mathbf{w}_t\right), \tag{2.28}$$

$$\mathbf{w}_{ttt}=-\partial_x\left(\mathbf{w}_t^T\cdot H\mathbf{f}\cdot\mathbf{w}_t+J\mathbf{f}\cdot\mathbf{w}_{tt}\right), \tag{2.29}$$

where $(J\mathbf{f})_{i,j}=\partial f_i/\partial u_j$ is the Jacobian of $\mathbf{f}$, while $(H\mathbf{f})_{i,j,k}=\partial^2 f_k/\partial u_j\partial u_i$ is the tensor of second derivatives. These formulas become even more complicated if the *Timeux* strategy is used.

Thus for the $m=4$ *Timed* scheme we need three piecewise polynomial interpolations for each component.

For the NCE Runge–Kutta (NCERK) scheme, we must compute all components of the approximate Runge–Kutta fluxes $g_i^{(j)}, i=1,\dots,M$, before computing the successive fluxes $g_i^{(j+1)}$. As for the *Timed* scheme, the method requires $m-1$ interpolations for each component, but no differentiation of the flux function $\mathbf{f}$ is required.

We only need an estimate of the maximum characteristic velocity to satisfy the CFL condition.

3. Stability and truncation analysis.

3.1. Linear stability analysis.

In this section we report our results for the linear stability analysis of the different schemes we are proposing. The analysis has two purposes: identify the linearly stable central schemes and compute the critical Courant number of the scheme. The former information will be used as a guideline for the choice of the stencil in the nonlinear schemes. The results summarized here are described in detail in the proceeding [2].

Let us consider a generic central scheme of third and fourth order, applied to the linear equation

$$u_t + u_x = 0.$$

Such a scheme will take the form

$$\begin{aligned} \overline{w}^{n+1}_{j+\frac{1}{2}} = & \sum_{l=0}^{m-1} \left(\frac{1}{2}\right)^{l+1} \frac{1}{(l+1)!}[\tilde{D}^l_j(\overline{w}^n) + (-1)^l \tilde{D}^l_{j+1}(\overline{w}^n)] \\ & - \frac{\lambda}{6}\{[w^n_{j+1} + 4w^{n+\frac{1}{2}}_{j+1} + w^{n+1}_{j+1}] - [w^n_j + 4w^{n+\frac{1}{2}}_j + w^{n+1}_j]\}, \end{aligned} \tag{3.1}$$

where the discrete space derivatives of the field, $\tilde{D}^l_j$, are obtained from cell averages $\{\overline{w}^n_j\}$ by deconvolution (see (2.17)). We will also need the quantities D^l_j defined in (2.10), which also approximate the derivatives but are obtained from interpolation.

The explicit expressions of $\tilde{D}^l_j$ and D^l_j as functions of $\overline{w}^n$ can be easily written and depend on the particular stencil chosen. We shall consider separately third- and fourth-order schemes. We want to study the linear stability of central schemes with a fixed stencil.

The values $w^{n+\frac{1}{2}}_j$ and w^{n+1}_j are obtained from w^n_j by a suitable Runge–Kutta scheme, with or without its NCE. Moreover they depend on the particular stencil chosen through the expressions for the $\tilde{D}^l_j$'s and the D^l_j's.

The different stencils will be labeled by the value of $il(j) - j$, where $il(j)$ is the leftmost point of the stencil, as in section 2.2.

Since the stencil of third-order schemes is formed by four points, the possible stencils are (-2), (-1), and (0).

For fourth-order schemes the stencil contains five points. The possible stencils are (-3), (-2), (-1), and (0).

Now we are ready to express (3.1) in terms of $\overline{w}^n$. The details can be found in [2].

The amplification factor is obtained by computing the evolution of the initial data

$$\overline{w}^n_j = \rho^n \mathrm{e}^{ij\xi},$$

where $i^2 = -1$. By substituting such expression in the numerical scheme one obtains

$$\overline{w}^{n+1}_{j+\frac{1}{2}} = \rho_\lambda(\xi)\mathrm{e}^{i\xi/2}\overline{w}^n_j, \qquad \xi \in [0, 2\pi].$$

Stability is studied by analyzing the function

$$P_\lambda(\xi) = |\rho_\lambda(\xi)|^2.$$

Table 3.1
Stable stencils for third-order schemes.

Third-order schemes		
Scheme	Stencil	Stability region
*RK*2-2	$j-2, j-1, j, j+1$	$\lambda^* = 0.35099$
	$j-1, j, j+1, j+2$	$\lambda^* = 0.43403$
	$j, j+1, j+2$	unstable
*NCERK*2	$j-2, j-1, j, j+1$	$\lambda^* = 0.348086$
	$j-1, j, j+1, j+2$	$\lambda^* = 0.435831$
	$j, j+1, j+2, j+3$	unstable
Timeux	$j-2, j-1, j, j+1$	$\lambda^* = 1/2$
	$j-1, j, j+1, j+2$	$\lambda^* = 1/2$
	$j, j+1, j+2, j+3$	unstable
Tadmor	$j-1, j, j+1$	$\lambda^* = 0.5$
*TadRK*2	$j-1, j.j+1$	$\lambda^* = 3/7$
*TadRK*2-2	$j-1, j, j+1$	$\lambda^* = 3/7$

Table 3.2
Stable stencils for fourth-order schemes.

Fourth-order schemes		
Scheme	Stencil	Stability region
*RK*3-2	$j-3, j-2, j-1, j, j+1$	unstable
	$j-2, j-1, j, j+1, j+2$	$\lambda^* = 9/22$
	$j-1, j, j+1, j+2, j+3$	moder. unstable
	$j, j+1, j+2, j+3, j+4$	unstable
*NCERK*4	$j-3, j-2, j-1, j, j+1$	unstable
	$j-2, j-1, j, j+1, j+2$	$\lambda^* = 9/22$
	$j-1, j, j+1, j+2, j+3$	moder. unstable
	$j, j+1, j+2, j+3, j+4$	unstable
Timeux	$j-3, j-2, j-1, j, j+1$	unstable
	$j-2, j-1, j, j+1, j+2$	$\lambda^* = 1/2$
	$j-1, j, j+1, j+2, j+3$	moder. unstable
	$j, j+1, j+2, j+3, j+4$	unstable

Let λ^* be the maximum value of λ for which

$$\max_{0 \le \xi \le 2\pi} |P_\lambda(\xi)| \le 1. \tag{3.2}$$

We say that the scheme is stable if there exist $\lambda^* > 0$.

From the analysis of $P_\lambda(\xi)$ corresponding to the previous schemes one obtains the stability results summarized in Tables 3.1 and 3.2, for third- and fourth-order schemes, respectively. Scheme Tadmor is the third-order scheme described in [10].

The values of λ^* have been computed by solving an algebraic equation obtained from condition (3.2).

The results of the analysis have been confirmed by the numerical results obtained by the above schemes.

For third-order schemes based on Runge–Kutta, we find that stencil (-2) and (-1) are stable, and the stability region is slightly smaller than the one corresponding to scheme *Tadmor* and the schemes based on Taylor expansion. Stencil (0) is unstable.

For fourth-order schemes based on Runge–Kutta, only the central stencil (-2) is stable. Stencil (-1) is moderately unstable for $\lambda < 0.4251$, and this instability is observed only after long integration time. Stencil (-3) and (0) are unstable.

Note that for the third-order schemes based on ENO reconstruction there are two central stencils (i.e., (-2) and (-1)), and those are both stable. If equation $u_t - u_x = 0$

is considered, then the results for stencil (-2) and (-1) for third-order schemes are reversed. In the case of systems, because one does not want to do upwinding, the most restrictive CFL condition has to be used. For the fourth-order schemes based on ENO there is one central stencil, and it is stable. In both cases, therefore, the stability does not depend on the sign of the characteristic velocity.

3.2. Truncation error. The purpose of this section is to explain why it is necessary to use an m degree interpolation polynomial in the reconstruction step to obtain a method of order m.

We consider a set of data $\{\overline{w}_j^n\}$ defining the numerically computed values of the cell averages of an approximation to the solution of the conservation law (2.1) at time t^n. We apply the reconstruction operator introduced in section 2.2 to the data $\{\overline{w}_j^n\}$, obtaining the function $w(x, t^n) = \mathcal{R}(\overline{w}^n;\, x)$. Then our solutions can be written in the form

$$\begin{aligned}\overline{w}_{j+1/2}^{n+1} &= \frac{1}{h}\left[\int_0^{h/2} w(x_j + y, t^n)\, dy + \int_{-h/2}^{0} w(x_{j+1} + y, t^n)\, dy\right] \\ &\quad -\frac{1}{h}\sum_{\ell=0}^{L} k[f(w(x_{j+1}, t^n + \tau_\ell)) - f(w(x_j, t^n + \tau_\ell))]\,\omega_\ell, \qquad (3.3)\end{aligned}$$

where $w(\cdot, t^n + \tau_\ell)$ are the values of $w(\cdot, t)$ evaluated on the nodes of the quadrature formula through a suitable Runge–Kutta scheme (section 2.4) or via Taylor expansion (section 2.3).

From now on we let $u(x, t)$ and $w(x, t)$ denote the exact solution of (2.1) and the numerical solution obtained by (3.3). We study the error produced by one time step; i.e., we suppose that the cell averages are exact at time t^n, namely, $\overline{w}_j^n = \overline{u}_j^n, j = 0, \dots$.

We recall that the reconstructed solution at time t^n is given by (2.18):

$$w(x, t^n) = \sum_{\ell=0}^{r} \frac{1}{l!}\tilde{D}_j^l \frac{(x - x_j)^l}{h^l}, \quad x \in I_j \equiv (x_{j-h/2}, x_{j+h/2}). \qquad (3.4)$$

In this section the $\tilde{D}_j^l$'s are approximations of the exact derivatives defined in (2.17). By construction they satisfy

$$\tilde{D}_j^\ell = h^\ell \left.\frac{\partial^l u}{\partial x^\ell}\right|_{x_j} + h^{R+1} e_{j,\ell}(x) + O(h^{R+2}) \qquad (3.5)$$

for a suitable R. If u is smooth enough, one can assume that the functions $e_{j,\ell}$'s are at least piecewise continuous. The index R (accuracy of the computed derivatives) and r (degree of the reconstructed polynomials) need not coincide. In our computations we will actually use $R = m$ and $r = m - 1$.

The error due to the time step of the scheme in the $(j+1/2)$th cell can be written as

$$\frac{\overline{u}_{j+1/2}^{n+1} - \overline{w}_{j+1/2}^{n+1}}{k} = E_S - E_T,$$

where $\overline{u}_{j+1/2}^{n+1} = \overline{u}(x_{j+1/2}, t^n + k)$, and E_S and E_T are the space and time contributions to the error, respectively, namely,

$$E_S = \frac{1}{kh}\left(\int_0^{h/2} u(x_j + y, t^n)\, dy - \int_0^{h/2} w(x_j + y, t^n)\, dy\right.$$

$$+ \int_{-h/2}^{0} u(x_{j+1}+y,t^n)\,dy - \int_{-h/2}^{0} w(x_{j+1}+y,t^n)\,dy\Bigg) \tag{3.6}$$

while

$$\begin{aligned} E_T = \frac{1}{kh}\Bigg(&\int_0^k [(f(u(x_{j+1},t^n+\tau)) - f(u(x_j,t^n+\tau))]\,d\tau \\ &- \sum_{\ell=0}^{L} k\,[f(w(x_{j+1},t^n+\tau_\ell)) - f(w(x_j,t^n+\tau_\ell))]\,\omega_\ell\Bigg). \end{aligned} \tag{3.7}$$

Here we used the fact that u solves exactly the weak form of the PDE on the cell $(x_{j-1/2},x_{j+1/2})\times(t^n,t^n+k)$.

Space contribution. We start from the space contribution. Substituting u with its Taylor expansion and w with (3.4) and integrating, we find

$$\begin{aligned} E_S = \frac{1}{kh}\Bigg(&\sum_{\ell=0}^{\infty}\frac{1}{(\ell+1)!}\left.\frac{\partial^\ell u}{\partial x^\ell}\right|_{x_j}\left(\frac{h}{2}\right)^{\ell+1} - \sum_{\ell=0}^{r}\frac{1}{(\ell+1)!}\tilde{D}_j^\ell\left(\frac{1}{2}\right)^{\ell+1} h \\ &- \sum_{\ell=0}^{\infty}\frac{1}{(\ell+1)!}\left.\frac{\partial^\ell u}{\partial x^\ell}\right|_{x_{j+1}}\left(-\frac{h}{2}\right)^{\ell+1} + \sum_{\ell=0}^{r}\frac{1}{(\ell+1)!}\tilde{D}_{j+1}^\ell\left(-\frac{1}{2}\right)^{\ell+1} h\Bigg). \end{aligned}$$

We substitute (3.5) into the $\tilde{D}_j^\ell$'s. Next, rearranging and keeping only higher order terms, we have

$$\begin{aligned} E_S = \frac{1}{\lambda}\Bigg[&\frac{1}{(r+2)!}\left(\frac{h}{2}\right)^r\left(\left.\frac{\partial^{r+1}u}{\partial x^{r+1}}\right|_{x_j} - (-1)^r\left.\frac{\partial^{r+1}u}{\partial x^{r+1}}\right|_{x_{j+1}}\right) \\ &- h^R\sum_{\ell=0}^{r}\frac{1}{2^{\ell+1}(\ell+1)!}\left(e_{j,\ell} - (-1)^{\ell+1}e_{j+1,\ell}\right)\Bigg] + O(h^{R+1}) + O(h^{r+1}), \end{aligned}$$

where we have used the fact that $kh = \lambda h^2$. The first term gives a contribution

$$\begin{aligned} &O(h^r) \text{ if } r \text{ is odd,} \\ &O(h^{r+1}) \text{ if } r \text{ is even.} \end{aligned}$$

The second term gives a contribution of order $O(h^R)$. Thus, if we want a method of order m we must have

$$R = m, \quad r = \begin{cases} m-1, & m \text{ odd,} \\ m, & m \text{ even.} \end{cases}$$

Our accuracy tests show that the requirement $R = m$ is strict, while r can be chosen as $r = m-1$ in all cases. This shows that the estimate may be too pessimistic in the evaluation of the number of terms needed in the Taylor expansion. However, the cost of the scheme depends more on the value of R, which must be chosen equal to m, and for this value the estimate is sharp.

Note that the space contribution to the error is entirely due to the staggered grid. Upwind schemes do not need cell staggering and for them $E_S = 0$. In central schemes, however, it is precisely E_S that introduces the stabilizing effect that counterbalances the negative diffusion characteristic of central differencing. Since our scheme is not symmetric (i.e., the stencil selection may be different at neighboring points and the same holds for the MinMod switch) the functions $e^n_{j,\ell}$ and $e^n_{j+1,\ell}$ do not in general cancel out. Therefore, we are forced to use an m-degree interpolation to obtain an m-order scheme. Moreover, even if the scheme is symmetric, $e_{j,\ell}$ and $e_{j+1,\ell}$ in general will not cancel out if the grid is not uniform.

Time contribution. We write the time contribution E_T to the truncation error (3.7) as the sum of the two contributions at x_j and x_{j+1}, namely, $E_T = -E_{T,j} + E_{T,j+1}$, where $E_{T,j}$ has been written as

$$\begin{aligned} E_{T,j} &= \frac{1}{kh}\left[\int_0^k f(u(x_j, t^n+\tau)) - \sum_{\ell=0}^{L} kf(u(x_j,t^n+\tau_\ell))\omega_\ell\right] \\ &\quad + \frac{1}{kh}\sum_{\ell=0}^{L}\left[kf(u(x_j,t^n+\tau_\ell)) - kf(w(x_j,t^n+\tau_\ell))\right]\omega_\ell \\ &= E_{T_1,j} + E_{T_2,j}. \end{aligned}$$

E_{T_1} is the error due to the quadrature formula. Since we are using Simpson's rule, the error due to the quadrature formula is $O(k^5)$ for each of the two time integrals appearing in $E_{T,j}$ and $E_{T,j+1}$. Because of cancellation we find that $E_{T_1} = -E_{T_1,j} + E_{T_1,j+1} = O(k^6)/(kh) = O(k^4)$.[1] Next we evaluate $E_{T_2,j}$. In the following we consider only the evaluation of $u(\cdot, t^n+\tau_\ell)$ via Taylor expansion; that is, we study the *Timeux* strategy of section 2.3. We have

$$E_{T_2,j} = E^{(1)}_{T_2,j} + E^{(2)}_{T_2,j}$$

with

$$\begin{aligned} E^{(1)}_{T_2,j} &= \frac{1}{kh}\sum_{\ell=0}^{L} k\left[f(u(x_j,t^n+\tau_\ell)) - f\left(\sum_{i=0}^{m-1}\frac{\tau_\ell^i}{i!}\left.\frac{\partial^i u}{\partial t^i}\right|_{(x_j,t^n)}\right)\right] \\ &= \frac{1}{kh}\sum_{\ell=0}^{L} kO(\tau_\ell^m) = O(k^{m-1}). \end{aligned}$$

If the grid is uniform, subtracting $E^{(1)}_{T_2,j+1} - E^{(1)}_{T_2,j}$ we gain one order, because f and u are smooth functions; therefore, $E^{(1)}_{T_2} = O(k^m)$. We now consider

$$E^{(2)}_{T_2,j} = \frac{1}{kh}\sum_{\ell=0}^{L} k\left[f\left(\sum_{i=0}^{m-1}\frac{\tau_\ell^i}{i!}\left.\frac{\partial^i u}{\partial t^i}\right|_{(x_j,t^n)}\right) - f\left(\sum_{i=0}^{m-1}\frac{\tau_\ell^i}{i!}\left.\frac{\partial^i w}{\partial t^i}\right|_{(x_j,t^n)}\right)\right],$$

where we have substituted $w(x_j, t^n+\tau_\ell)$ with its Taylor expansion. If we use a reconstruction based on a polynomial of degree $R = m$, and we apply (3.5), we find

$$\tau_\ell^i\frac{\partial^i u}{\partial t^i} = \tau_\ell^i\frac{\partial^i w}{\partial t^i} + O(h^{m+1}).$$

Time derivatives of w are computed by *Timeux* strategy, by making use of the equation. We therefore find

$$E^{(2)}_{T_2,j} = \frac{1}{kh}\sum_{\ell=0}^{M} kO(h^{m+1}) = O(h^m).$$

[1] This is enough for both $m = 3$ and $m = 4$. For more accurate schemes Simpson's rule is not enough.

If $E^{(2)}_{T_2,j}$ and $E^{(2)}_{T_2,j+1}$ cancel out we can use a lower degree polynomial, namely, $R = m - 1$. However, if the grid is not uniform, and/or the scheme is not symmetric around $x_{j+1/2}$, this cancellation may not hold, and a reconstruction of degree $R = m$ becomes necessary.

Accuracy of Tadmor scheme. We noted that an m-degree interpolation is needed in order to obtain an m-order accurate method. Usually, however, we expect that a polynomial of degree $m - 1$ should be enough for a uniform grid.

The extra computational effort required by our schemes is due to the high nonlinearity of the reconstruction scheme. We illustrate this problem by computing the space contribution to the truncation error (E_S) for Tadmor's third-order scheme, as defined in [10]. We start from the definition of E_S given in (3.6), but now $w(x, t^n)$ is obtained starting from the cell averages $\{\overline{w}^n_j\}$ with Tadmor's third-order NED reconstruction, namely,

$$w(x,t^n)|_{I_j} = \overline{w}^n_j + \theta_j(q_j(x) - \overline{w}^n_j), \qquad 0 < \theta_j \leq 1,$$

where θ_j is the flux limiter, see [10], and $q_j(x)$ is the second degree interpolant of the cell averages, namely,

$$q_j(x) = \overline{w}^n_j - \frac{1}{24}\Delta^2\overline{w}^n_j + \Delta_0\overline{w}^n_j\left(\frac{x - x_j}{h}\right) + \frac{1}{2}\Delta^2\overline{w}^n_j\left(\frac{x - x_j}{h}\right)^2,$$

where

$$\begin{aligned}\Delta_0 w(x) &= \frac{1}{2}(w(x+h) - w(x-h)),\\ \Delta^2 w(x) &= w(x+h) - 2w(x) + w(x-h).\end{aligned}$$

We define the integrals of the initial conditions, S_1 and S_2, as follows:

$$\begin{aligned}S_1 &= \int_0^{h/2} w(x_j + y, t^n)\,dy = \overline{w}_j\frac{h}{2} + \frac{h}{16}\theta_j(\overline{w}_{j+1} - \overline{w}_{j-1}),\\ S_2 &= \int_{-h/2}^{0} w(x_{j+1} + y, t^n)\,dy = \overline{w}_{j+1}\frac{h}{2} - \theta_{j+1}\frac{h}{16}(\overline{w}_{j+2} - \overline{w}_j).\end{aligned}$$

Let us consider S_1. We compute the cell averages $\overline{w}_\ell = \overline{u}_\ell$, $\ell = j-1, j, j+1$ in terms of the derivatives of u at x_j. Expanding u in a power series we find

$$\overline{w}^n_j = \frac{1}{h}\int_{-h/2}^{h/2} u(x_j + y)\,dy = \frac{1}{h}\sum_{\ell=0}^{\infty}\frac{1}{(\ell+1)!}\left.\frac{\partial^\ell u}{\partial x^\ell}\right|_{x_j}\left(\frac{h}{2}\right)^{\ell+1}\alpha_{\ell+1},$$

where

$$\alpha_{\ell+1} = 1 - (-1)^{\ell+1}.$$

Similarly

$$\begin{aligned}\overline{w}^n_{j+1} &= \frac{1}{h}\sum_{\ell=0}^{\infty}\frac{1}{(\ell+1)!}\left.\frac{\partial^\ell u}{\partial x^\ell}\right|_{x_j}\left(\frac{h}{2}\right)^{\ell+1}(3^{\ell+1} - 1),\\ \overline{w}^n_{j-1} &= \frac{1}{h}\sum_{\ell=0}^{\infty}\frac{1}{(\ell+1)!}\left.\frac{\partial^\ell u}{\partial x^\ell}\right|_{x_j}\left(\frac{h}{2}\right)^{\ell+1}((-1)^{\ell+1} - (-3)^{\ell+1}).\end{aligned}$$

We substitute the expansion for the cell averages in S_1 and we compute

$$\begin{aligned} E_{S_1} &= \frac{1}{kh}\left[\int_0^{h/2} u(x_j+y,t^n)\,dy - \int_0^{h/2} w(x_j+y,t^n)\,dy\right] \\ &= \frac{1}{k}\left\{\sum_{\ell=0}^{3} c_\ell^+ \left.\frac{\partial^\ell u}{\partial x^\ell}\right|_{x_j}\left(\frac{h}{2}\right)^\ell + O(h^4)\right\}. \end{aligned}$$

Elementary calculations show that

$$\begin{aligned} c_0^+ &= 0, \qquad & c_1^+ &= \frac{1}{2}(1-\theta_j), \\ c_2^+ &= 0, \qquad & c_3^+ &= \frac{1}{4!}(1-10\theta_j). \end{aligned}$$

Similarly, expanding around x_{j+1},

$$\begin{aligned} E_{S_2} &= \frac{1}{kh}\left[\int_{-h/2}^{0} u(x_{j+1}+y,t^n)\,dy - \int_{-h/2}^{0} w(x_{j+1}+y,t^n)\,dy\right] \\ &= \frac{1}{k}\left\{\sum_{\ell=0}^{3} c_\ell^- \left.\frac{\partial^\ell u}{\partial x^\ell}\right|_{x_{j+1}}\left(\frac{h}{2}\right)^\ell + O(h^4)\right\}, \end{aligned}$$

where

$$\begin{aligned} c_0^- &= 0, \qquad & c_1^- &= \frac{1}{2}(1-\theta_{j+1}), \\ c_2^- &= 0, \qquad & c_3^- &= \frac{1}{4!}(1-10\theta_{j+1}). \end{aligned}$$

Note that if $\theta_j = 1 + O(h^2)$ then both E_{S_1} and E_{S_2} are $O(h^2)$. Adding the previous expressions we find

$$\begin{aligned} E_{S_1}+E_{S_2} &= \frac{1}{k}\left\{\left[\frac{1}{2}(1-\theta_j)\left.\frac{\partial u}{\partial x}\right|_{x_j} - \frac{1}{2}(1-\theta_{j+1})\left.\frac{\partial u}{\partial x}\right|_{x_j+1}\right]\frac{h}{2}\right. \\ &\quad \left. + \left(\frac{h}{2}\right)^3\left[\frac{1}{4!}(1-10\theta_j)\left.\frac{\partial^3 u}{\partial x^3}\right|_{x_j} - \frac{1}{4!}(1-10\theta_{j+1})\left.\frac{\partial^3 u}{\partial x^3}\right|_{x_{j+1}}\right]\right\} \\ &= \frac{1}{k}(\theta_{j+1}-\theta_j)\left.\frac{\partial u}{\partial x}\right|_{\xi}\frac{h}{2} + \frac{10}{4!k}(\theta_{j+1}-\theta_j)\left.\frac{\partial^3 u}{\partial x^3}\right|_{\eta}\left(\frac{h}{2}\right)^3 + O(h^3), \end{aligned}$$

where $\xi, \eta \in (x_j, x_{j+1})$. If $\theta_j \equiv 1$ and the grid is uniform the method is $O(h^3)$. If the grid is not uniform, and the change in the grid size is not smooth, then the method is $O(h^2)$. If θ_j oscillates without continuity the method is not third-order accurate, even on a uniform grid. Summarizing, the scheme is third order provided the grid is uniform or varies smoothly, and $\theta_j = 1 + O(h)$ and varies smoothly.

We see therefore that if θ_j is not regular enough, accuracy deteriorates, as is apparent in the results obtained in section 4.1 with the scheme *TadRK*. On the other hand, for our schemes, E_{S_1} and E_{S_2} are each $O(h^{m+1})$. Thus we do not have to rely on cancellation to obtain a method of order m. This of course is obtained with the use of an m-degree polynomial in the reconstruction. However, the extra effort in the reconstruction is compensated by the robustness of the accuracy.

4. Numerical results. In this section we first compare our third-order schemes with central schemes based on Tadmor's third-order NED reconstruction on a single scalar equation. Next we test our fourth-order schemes. We conclude the discussion of the scalar equation addressing the crucial point of the choice of the stencil. Our results show that *Timeux* with the MC stencil and *NCERK* with the MC stencil are accurate, robust, and efficient third- and fourth-order shock capturing schemes.

Finally, we consider the application of our schemes to systems of conservation laws. In this case, we show only results obtained with *NCERK* schemes which are particularly suited for systems of equations, as discussed in section 2.5.

4.1. Scalar equation. We study the performance of our schemes by using three test cases.

Test 1.

$$\begin{array}{l} u_t + u_x = 0, \\ u(x,t=0) = \sin(\pi x), \\ \text{periodic boundary conditions on } [-1,1], \\ \text{integration time: } T = 10. \end{array}$$

This test is used to check the convergence rate at large times.

Test 2.

$$\begin{array}{l} u_t + u_x = 0, \\ u(x,t=0) = \sin^4(\pi x), \\ \text{periodic boundary conditions on } [-1,1], \\ \text{integration time: } T = 1. \end{array}$$

This test is used to detect possible deterioration of accuracy due to strong oscillations in the parameters that determine the stencil (such as in ENO schemes) or the flux limiter (such as in *TadRK*).

Test 3.

$$\begin{array}{l} u_t + (\frac{1}{2}u^2)_x = 0, \\ u(x,t=0) = 1 + \frac{1}{2}\sin(\pi x), \\ \text{periodic boundary conditions on } [-1,1], \\ \text{integration times: } T = 0.33 \text{ and } T = 1.5. \end{array}$$

Here $T = 0.33$ is chosen for convergence tests and $T = 1.5$ for shock capturing tests. (Note that the shock develops at $T_s = 2/\pi \simeq 0.7$.)

Let $u(x,t^n)$ and w_j^n be the exact solution and the computed solution, respectively, at (x_j,t^n). Then the norms of the error are given by

$$\begin{array}{lll} L^1 & \text{error :} & ||u-w||_1 = \sum_{j=1}^N |u(x_j,t^n) - w_j^n| h, \\ L^\infty & \text{error :} & ||u-w||_\infty = \max_{1\le j\le N} |u(x_j,t^n) - w_j^n|. \end{array}$$

Third-order schemes. We compare the following schemes.

1. *Tadmor*: it is the third-order scheme described in [10].
2. *TadRK*: it is based on Tadmor's piecewise quadratic third-order reconstruction, and the computation of the flux is performed with a second-order Runge–Kutta method, coupled with its NCE.
3. *NCERK*2: this scheme is based on ENO reconstruction, and the time evolution is computed by a second-order Runge–Kutta scheme with NCE.
4. *Timeux*: it is as in *NCERK*, but with the time evolution computed via Taylor expansion.

Table 4.1
Third-order schemes.

Scheme	Reconstruction	Flux evaluation	Stencil selection
Tadmor	NED, $r = 2$	Taylor expansion	
TadRK	NED, $r = 2$	RK2 + NCE	
*NCERK*2	ENO, $r = 3$	RK2 + NCE	MC, Shu, HEOC
Timeux	ENO, $r = 3$	Taylor expansion	MC, Shu, HEOC

Table 4.2
Accuracy Test 1*. Scheme Tadmor has* $\lambda = 0.45$*; the others have* $\lambda = 3/7 * .9$*. MC stencil.*

Linear advection, $T = 10, u_0(x) = \sin(\pi x), m = 3$

N	Tadmor	TadRK	Timeux	NCERK2
	L^1 error			
20	0.1101E-01	0.3791E-01	0.7921E-02	0.1387E-01
40	0.1384E-02	0.4778E-02	0.5409E-03	0.1483E-02
80	0.1730E-03	0.6023E-03	0.3813E-04	0.1799E-03
160	0.2185E-04	0.7512E-04	0.3187E-05	0.2229E-04
320	0.2731E-05	0.9390E-05	0.3509E-06	0.2774E-05
640	0.3413E-06	0.1174E-05	0.4236E-07	0.3463E-06
	L^1 order			
20	-	-	-	-
40	2.9925	2.9879	3.8721	3.2252
80	2.9998	2.9880	3.8264	3.0436
160	2.9847	3.0032	3.5805	3.0125
320	3.0004	2.9999	3.1835	3.0065
640	3.0002	3.0000	3.0503	3.0020

Table 4.3
Accuracy Test 1*. Scheme Tadmor has* $\lambda = 0.45$*; the others have* $\lambda = 3/7 * 0.9$*. MC stencil.*

Linear advection, $T = 10, u_0(x) = \sin(\pi x), m = 3$

N	Tadmor	TadRK	Timeux	NCERK2
	L^∞ error			
20	0.8567E-02	0.2931E-01	0.9511E-02	0.1553E-01
40	0.1084E-02	0.3738E-02	0.1085E-02	0.1921E-02
80	0.1358E-03	0.4725E-03	0.1234E-03	0.2293E-03
160	0.1716E-04	0.5898E-04	0.1382E-04	0.2710E-04
320	0.2145E-05	0.7374E-05	0.1552E-05	0.3210E-05
640	0.2681E-06	0.9218E-06	0.1742E-06	0.3817E-06
	L^∞ order			
20	-	-	-	-
40	2.9824	2.9711	3.1313	3.0151
80	2.9972	2.9836	3.1363	3.0666
160	2.9840	3.0021	3.1586	3.0813
320	3.0002	2.9997	3.1551	3.0775
640	3.0002	3.0000	3.1550	3.0721

The different schemes are summarized in Table 4.1, where r denotes the degree of the piecewise polynomial used in the reconstruction. We perform several runs with different grid sizes and evaluate error and convergence rate. For each scheme we select a value of $\lambda = \Delta t/\Delta x$ that satisfies the linear stability condition. *NCERK*2 and *Timeux* have the *MC* stencil.

The results for Test 1 are summarized in Tables 4.2 and 4.3. *Timeux* appears to be most accurate; however, Tadmor's original scheme is less expensive because it uses piecewise parabolic reconstruction, instead of a piecewise cubic reconstruction, and it enjoys a slightly less restrictive CFL condition ($\lambda = 0.9 * 1/2$ versus $\lambda = 0.9 * 3/7$).

TABLE 4.4

Accuracy Test 2. Scheme Tadmor has $\lambda = 0.45$; TadRK has $\lambda = 0.5 * (3/7 * 0.9)$; the others have $\lambda = 3/7 * 0.9$. NCERK and Timeux have the MC stencil.*

Linear advection, $T = 1, u_0(x) = \sin^4(\pi x), m = 3$

N	Tadmor	TadRK	TadRK*	Timeux	NCERK2
			L^1 error		
20	0.2339E-01	0.6750E-01	0.1706	0.3025E-01	0.4466E-01
40	0.3594E-02	0.1035E-01	0.3172E-01	0.2777E-02	0.6076E-02
80	0.5001E-03	0.1553E-02	0.5412E-02	0.2929E-03	0.6403E-03
160	0.8388E-04	0.2729E-03	0.7241E-03	0.2137E-04	0.7415E-04
320	0.1543E-04	0.1603E-03	0.1046E-03	0.1665E-05	0.9084E-05
640	0.2746E-05	0.4894E-04	0.1748E-04	0.1631E-06	0.1129E-05
			L^1 order		
20	-	-	-	-	-
40	2.7021	2.7054	2.4272	3.4452	2.8777
80	2.8453	2.7366	2.5509	3.2453	3.2465
160	2.5758	2.5084	2.9019	3.7770	3.1102
320	2.4422	0.7678	2.7915	3.6821	3.0290
640	2.4908	1.7114	2.5806	3.3516	3.0083

The results of Test 2 are shown in Table 4.4 for the L^1 norm. We observe that both *Timeux* and *NCERK*2 are fully third-order accurate, while a deterioration of accuracy appears on NED-based schemes, especially on *TadRK*. This phenomenon can be partly reduced by using a smaller time step (see the column labeled TadRK*). This effect is associated with the presence of strong oscillations in the flux limiter θ that appears in the NED reconstruction.

If θ is set to 1, i.e., if we use a fixed centered stencil, full third-order accuracy is recovered. The oscillations in θ decrease in time, and they are more pronounced on fine grids. Figure 4.1 shows the oscillations in the flux limiter at time $t = 0.5$ for *TadRK*. Two different grid sizes are shown. We can see clearly that a smaller time step dampens the oscillations.

Next we consider the convergence results for the Burgers equation at $T = 0.33$. Once more, *Timeux* and *NCERK*2 are fully third-order methods both in L^1 and L^∞. The results in the L^1 norm are shown in Table 4.5. Again, a deterioration of accuracy is apparent in *TadRK*, which is mitigated if λ is reduced well below the linear stability critical value. We obtain similar results in the L^∞ norm.

We conclude this accuracy comparison noting that our third-order *Timeux* scheme is comparable with Tadmor's scheme, because it yields smaller errors in all tests considered. We believe this compensates for the fact that it is slightly more expensive. On the other hand, scheme *NCERK*2 is superior to its NED analogue, *TadRK*, because it is more robust.

Fourth-order schemes. We now compare our fourth-order schemes. Tables 4.6, 4.7, and 4.8 contain the data for Test 1, Test 2, and Test 3, respectively. As already noted in section 2.4, the most economical version of *NCERK* in this case requires an RK scheme of order 4. All data shown were obtained with the MC stencil.

We note that in all test cases our schemes are even more than fourth-order accurate. Moreover, the error is much smaller than third-order schemes, even on the coarsest mesh. This extra improvement with respect to the $m = 3$ case can be probably explained in part with the symmetry of the $m = 4$ stencil. In the $m = 3$ case, the stencil of the polynomial interpolant consists of four points which cannot be symmet-

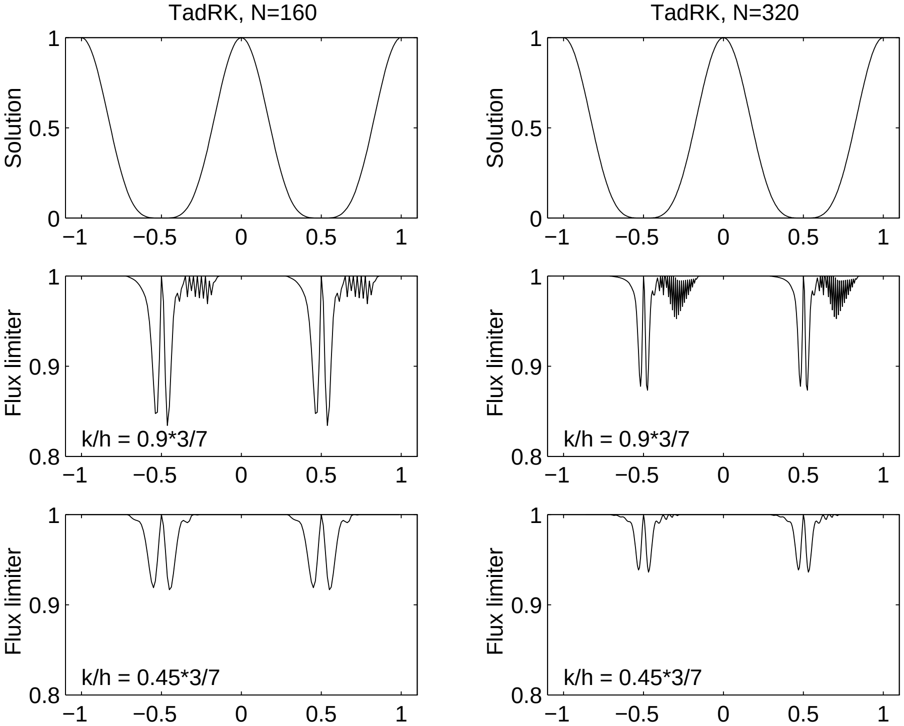

FIG. 4.1. *Flux limiter θ for scheme TadRK in Test* 2 *at $t = 0.5$.*

TABLE 4.5

Accuracy Test 3. *Scheme Tadmor has $\lambda = 0.33$; TadRK* has $\lambda = 0.5 * (3/7 * 0.66)$; the others have $\lambda = 3/7 * 0.66$. NCERK and Timeux have the MC stencil.*

Burgers's equation, $T = .33, u_0(x) = 1 + \frac{1}{2}\sin(\pi x), m = 3$

N	Tadmor	TadRK	TadRK*	Timeux	NCERK2
			L^1 error		
20	0.2195E-02	0.3342E-02	0.7259E-02	0.1429E-02	0.1538E-02
40	0.3145E-03	0.5096E-03	0.1132E-02	0.1229E-03	0.1446E-03
80	0.4330E-04	0.9011E-04	0.1770E-03	0.9969E-05	0.1514E-04
160	0.5862E-05	0.4031E-04	0.2708E-04	0.9395E-06	0.1643E-05
320	0.7788E-06	0.4718E-04	0.4730E-05	0.8835E-07	0.1869E-06
640	0.1073E-06	0.1404E-04	0.9078E-06	0.9433E-08	0.2179E-07
			L^1 order		
20	-	-	-	-	-
40	2.8034	2.7135	2.6812	3.5392	3.4114
80	2.8606	2.4995	2.6766	3.6244	3.2557
160	2.8849	1.1605	2.7085	3.4075	3.2037
320	2.9121	-0.2269	2.5174	3.4106	3.1367
640	2.8590	1.7490	2.3815	3.2274	3.1004

rically distributed around the base point. Since in a central scheme we cannot bias the stencil selection on the characteristic direction, we arbitrarily chose a left bias for the central stencil. The scheme might improve if this bias were changed at each time step. Furthermore, the ODE solver is comparatively more accurate than in the $m = 3$ case.

Table 4.6
Accuracy Test 1*. Timeux has* $\lambda = 3/7 * 0.9$*; NCERK*4 *has* $\lambda = 2/7 * 0.9$*. MC stencil.*

Linear advection, $T = 10, u_0(x) = \sin(\pi x), m = 4$

	Timeux		NCERK4	
N	L^1 error	L^1 order	L^1 error	L^1 order
20	0.7513E-03	-	0.2131E-02	-
40	0.2620E-04	4.8419	0.7699E-04	4.7905
80	0.9701E-06	4.7552	0.2923E-05	4.7192
160	0.4374E-07	4.4710	0.1387E-06	4.3970
320	0.2371E-08	4.2055	0.7798E-08	4.1529
640	0.1409E-09	4.0727	0.4719E-09	4.0467

Table 4.7
Accuracy Test 2*. Timeux has* $\lambda = 3/7 * .9$*; NCERK*4 *has* $\lambda = 2/7 * .9$*. MC stencil.*

Linear advection, $T = 1, u_0(x) = \sin^4(\pi x), m = 4$

	Timeux		NCERK4	
N	L^1 error	L^1 order	L^1 error	L^1 order
20	0.1469E-01	-	0.3921E-01	-
40	0.9947E-03	3.8842	0.2340E-02	4.0668
80	0.4115E-04	4.5953	0.8991E-04	4.7018
160	0.2032E-05	4.3399	0.4248E-05	4.4037
320	0.1164E-06	4.1260	0.2439E-06	4.1226
640	0.5855E-08	4.3131	0.1297E-07	4.2328

Table 4.8
Accuracy test 3*. Timeux has* $\lambda = 3/7 * 0.9$*; NCERK*4 *has* $\lambda = 2/7 * 0.9$*. MC stencil.*

Burgers's equation, $T = 0.33, u_0(x) = 1 + \frac{1}{2}\sin(\pi x), m = 4$

	Timeux		NCERK4	
N	L^1 error	L^1 order	L^1 error	L^1 order
20	0.1202E-02	-	0.1659E-02	-
40	0.7253E-04	4.0511	0.1195E-03	3.7948
80	0.2648E-05	4.7759	0.4706E-05	4.6671
160	0.9922E-07	4.7379	0.1817E-06	4.6946
320	0.4514E-08	4.4580	0.8004E-08	4.5048
640	0.2239E-09	4.3338	0.4016E-09	4.3169

Table 4.9
*NCERK*2 *with* $\lambda = 0.9 * (3/7)$*. Deterioration of accuracy with the Shu and HEOC stencils.*

Burgers's equation, $T = .33, u_0(x) = 1 + \frac{1}{2}\sin(\pi x), m = 3$

	Shu		HEOC	
N	L^∞ error	L^∞ order	L^∞ error	L^∞ order
20	0.4981E-02	-	0.6804E-02	-
40	0.8881E-03	2.4876	0.6714E-03	3.3410
80	0.1096E-03	3.0184	0.2962E-02	-2.1414
160	0.1177E-04	3.2190	0.4267E-02	-0.5267
320	0.1447E-02	-6.9413	0.2611E-02	0.7085
640	0.1345E-02	0.1050	0.5007E-03	2.3827

We obtain similar results with the equation $u_t - u_x = 0$ for both $m = 3$ and $m = 4$.

In the previous results, the stencil in *NCERK* and *Timeux* was chosen with the MC technique. We now show that other commonly used choices in upwind-based

Table 4.10

NCERK4 with $\lambda = 0.9 * (2/7)$. Deterioration of accuracy with the Shu and HEOC stencils.

Burgers's equation, $T = .33, u_0(x) = 1 + \frac{1}{2}\sin(\pi x), m = 4$

	Shu		HEOC	
N	L^∞ error	L^∞ order	L^∞ error	L^∞ order
20	0.4690E-02	-	0.3767E-02	-
40	0.7195E-03	2.7045	0.3155E-03	3.5775
80	0.1452E-03	2.3088	0.2832E-04	3.4780
160	0.4763E-04	1.6082	0.6485E-04	-1.1953
320	0.3416E-04	0.4796	0.4108E-04	0.6586
640	0.4586E-04	-0.4249	0.7215E-04	-0.8124

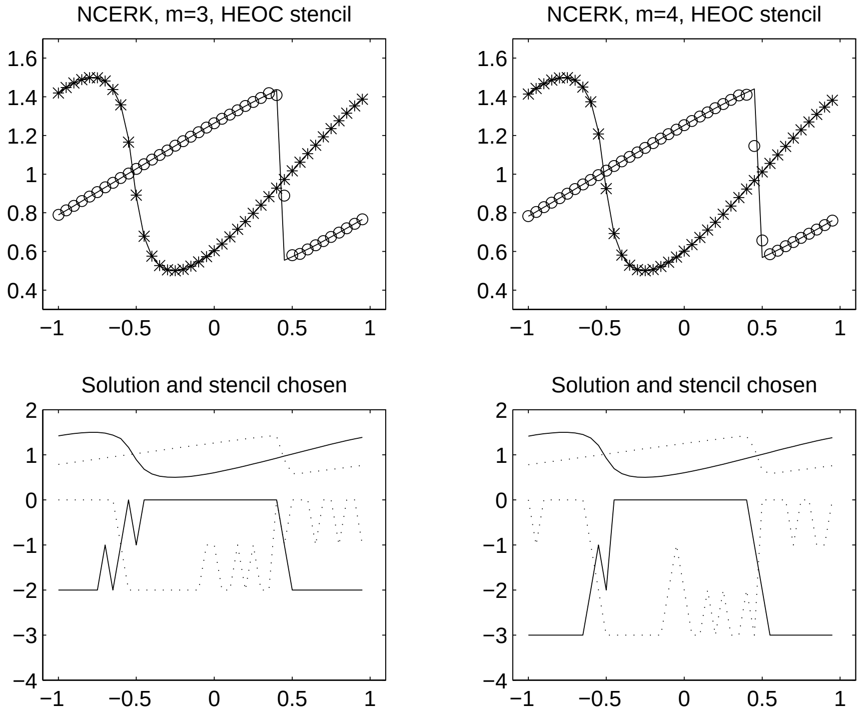

Fig. 4.2. *Solution of Test* 3 *and corresponding stencils at time $T = 0.5$ and $T = 1.5$.*

schemes perform poorly when coupled with our central schemes. More precisely, when the HEOC and Shu's stencil selections are applied to our *NCERK* schemes a deterioration of accuracy can be observed. These results are shown in Tables 4.9 and 4.10 for Test 3. Similar results are obtained also for Test 2.

A possible explanation of this pathological behavior can be found in the frequent choice of linearly unstable stencils by HEOC and Shu methods. This problem is illustrated in Figures 4.2 and 4.3, respectively, for the HEOC and Shu stencils on the Burgers equation. Figure 4.4 shows the corresponding results obtained with the MC stencil.

The solution is shown before and after shock formation for both $m = 3$ and $m = 4$. The bottom part of each figure superimposes the numerical solution to the stencil selected at each grid point. More precisely, we have plotted the function

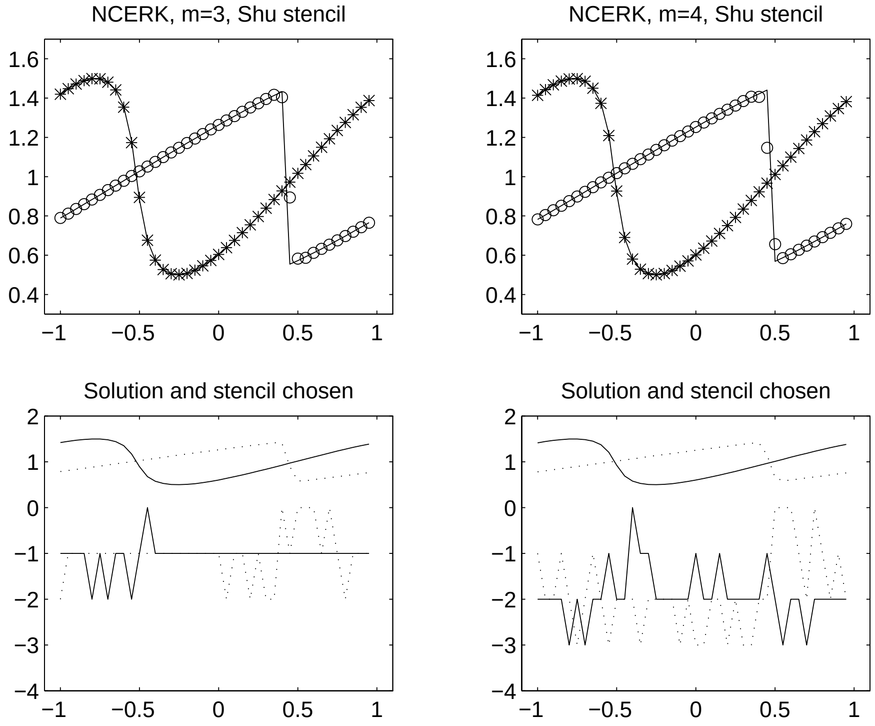

FIG. 4.3. *Solution of Test* 3 *and corresponding stencils at time* $T = 0.5$ *and* $T = 1.5$.

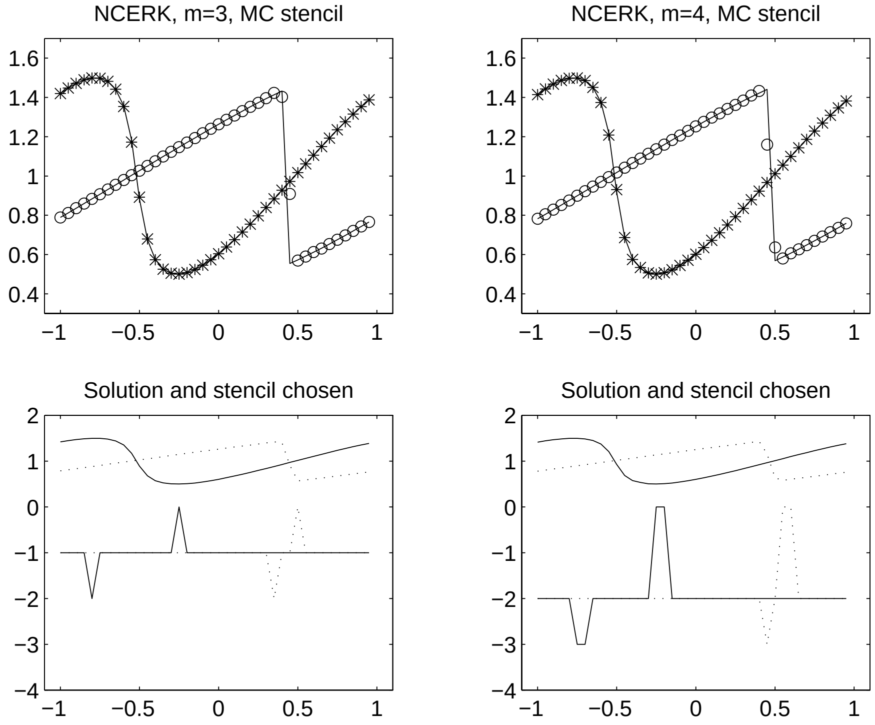

FIG. 4.4. *Solution of Test* 3 *and corresponding stencils at time* $T = 0.5$ *and* $T = 1.5$.

$s(j) = il(j) - j$, where $il(j)$ is the leftmost point of the stencil. (See section 2.2.) Thus $s(j) = 0$ corresponds to a stencil completely shifted to the right of the point x_j. The linearly stable selections are $s = -1$ and $s = -2$ for $m = 3$ and $s = -2$ for $m = 4$. (See section 3.1.)

In Figure 4.2, we see that the HEOC stencil selects frequently the linearly unstable positions. From Figure 4.3 we note that, although Shu's stencil spends less time in the linearly unstable positions, it oscillates rapidly, with very irregular behavior. Instead, Figure 4.4 shows that the MC stencil is always located on the linearly stable positions, unless a biased choice is necessary to prevent the onset of oscillations.

Note, however, that all three schemes present a sharp shock resolution, without oscillations.

4.2. Systems of equations. In this section we test our schemes on the system of Euler equations for a polytropic gas, with $\gamma = 1.4$. We consider the same test problems studied in [10]. Below we briefly restate the test problems for the sake of completeness. The variables ρ, m, E, and p denote the density, momentum, total energy per unit volume, and the pressure, respectively.

Test 4. Shock tube problem with Sod's initial data [17]:

$$\begin{cases} (\rho_l, m_l, E_l) = (1, 0, 2.5), & x < 0.5, \\ (\rho_r, m_r, E_r) = (0.125, 0, 0.25), & x > 0.5. \end{cases}$$

Test 5. Shock tube problem with the Lax initial data [5]:

$$\begin{cases} (\rho_l, m_l, E_l) = (0.445, 0.311, 8.928), & x < 0.5, \\ (\rho_r, m_r, E_r) = (0.5, 0, 1.4275), & x > 0.5. \end{cases}$$

In both cases the computational domain is $[0, 1]$; we integrate the equations up to $T = 0.16$, i.e., before the perturbations reach the boundary of the computational region (free flow boundary conditions). The computational parameters are $\lambda = 0.1$ and $N = 200$.

Test 6. Double blast wave by Woodward and Colella [18]:

$$\begin{cases} (\rho_l, m_l, p_l) = (1, 0, 1000), & x < 0.1, \\ (\rho_c, m_c, p_c) = (1, 0, 0.01), & 0.1 < x < 0.9, \\ (\rho_r, m_r, p_r) = (1, 0, 100), & x > 0.9. \end{cases}$$

In this case, the boundary is reflective at both ends. The equations are integrated up to $T = 0.038$, with $\lambda = 0.01$ and $N = 400$. By this time, the shock waves arising from the initial discontinuities have already collided, giving rise to a complex wave pattern. This structure is further complicated by the interactions with the reflected rarefaction waves.

All results shown are obtained with the *NCERK* scheme and the MC stencil.

Figure 4.5 contains the results obtained with Sod's initial data for $m = 3$ (*NCERK*2) and $m = 4$ (*NCERK*4). The solution obtained with $m = 3$ has some small oscillations that disappear for $m = 4$. Note also a slight improvement in the resolution of the contact discontinuity. (The transition occurs in seven points when $m = 3$ and in five points for $m = 4$.) Also the corners at the back and the front of the rarefaction are improved. There is no qualitative improvement in the resolution of the shock wave.

The improvement in the resolution of contact waves is more apparent in Figure 4.6 (the Lax test problem). We note that our *NCERK* schemes produce a sharp solution

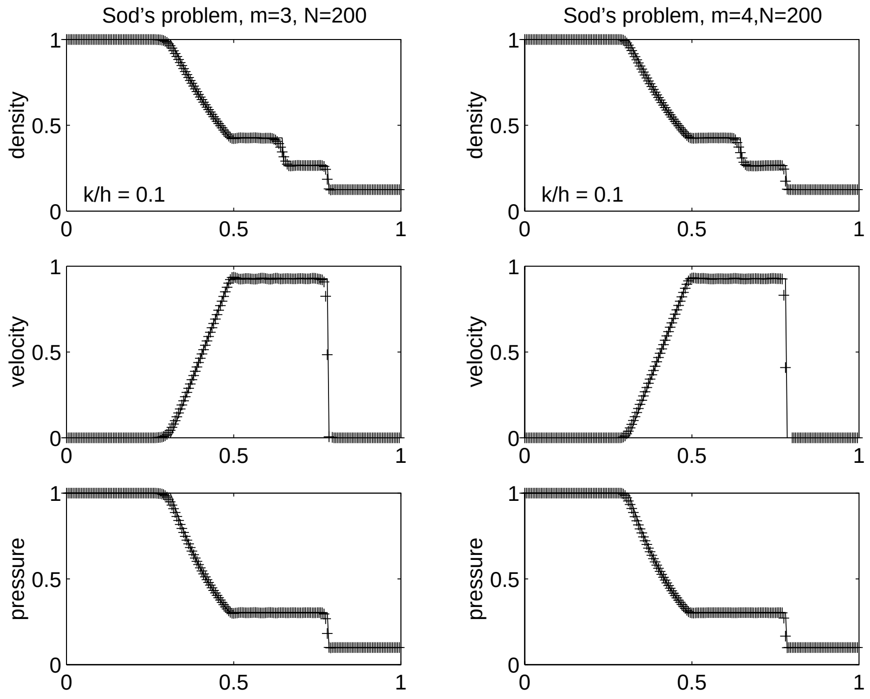

FIG. 4.5. *Solution of the Euler equations for Test* 4 *at time* $T = 0.16$.

on both contacts and shocks, at least in this case. There are some slight oscillations at the back of the rarefaction in the velocity field, but they remain bounded.

Figure 4.7 contains a further comparison between $NCERK2$ and $NCERK4$, for Test 6, at $T = 0.01$. The improvement in the resolution of the density peaks is noticeable. Comparing with the "exact" solution by Woodward and Colella, we see that when $m = 4$ the density peaks have almost the correct value (they should be both $\simeq 6$). Moreover, the rarefaction occurring on the left between the contact and the shock wave is well resolved for the $m = 4$ case.

There are some oscillations in the velocity and the pressure (especially for $m = 3$) which tend to diminish at later times. (Compare with Figure 4.8 for $m = 4$.)

Figure 4.8 shows the results obtained with the $NCERK4$ scheme at $T = 0.03$ and $T = 0.038$. We note that the small oscillations present before tend to disappear. As already noted, the ENO reconstruction is not enough to prevent local oscillations at the time of wave interactions. Such oscillations, however (if they do arise), tend to disappear as time increases, and the waves separate. Therefore, these oscillations are a temporary phenomenon, which does not trigger the choice of unphysical solutions or herald a breakdown in the computation.

On the other hand, high resolution of discontinuous solutions is maintained at all stages of the computation.

Conclusions. The central approach, combined with high-order ENO reconstruction and Runge–Kutta–NCE flux evaluation, provides accurate easy-to-use shock capturing schemes for conservation laws. The use of weighted ENO reconstruction may result in more efficient schemes (for the same accuracy). Such an approach has been tested in one dimension [7] and is used for two-dimensional extension of the method [8].

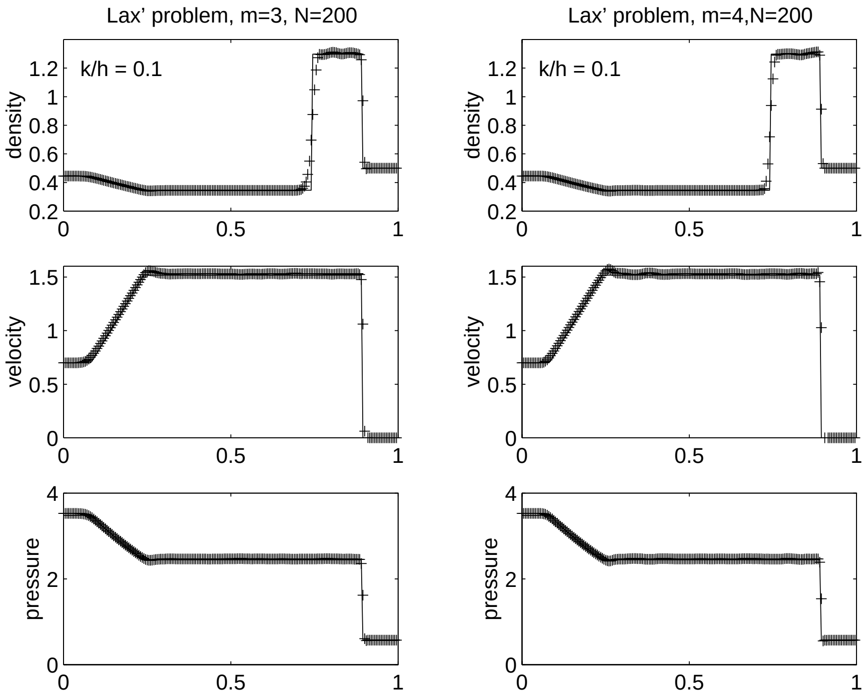

FIG. 4.6. *Solution of the Euler equations for Test* 5 *at time* $T = 0.16$.

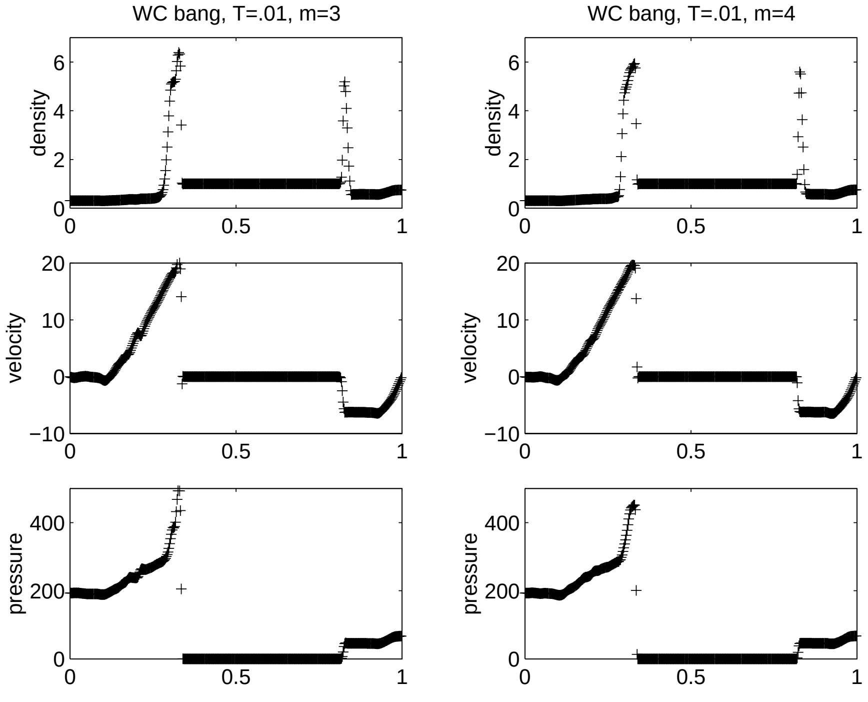

FIG. 4.7. *Solution of the Euler equations for Test* 6. $\lambda = 0.01$.

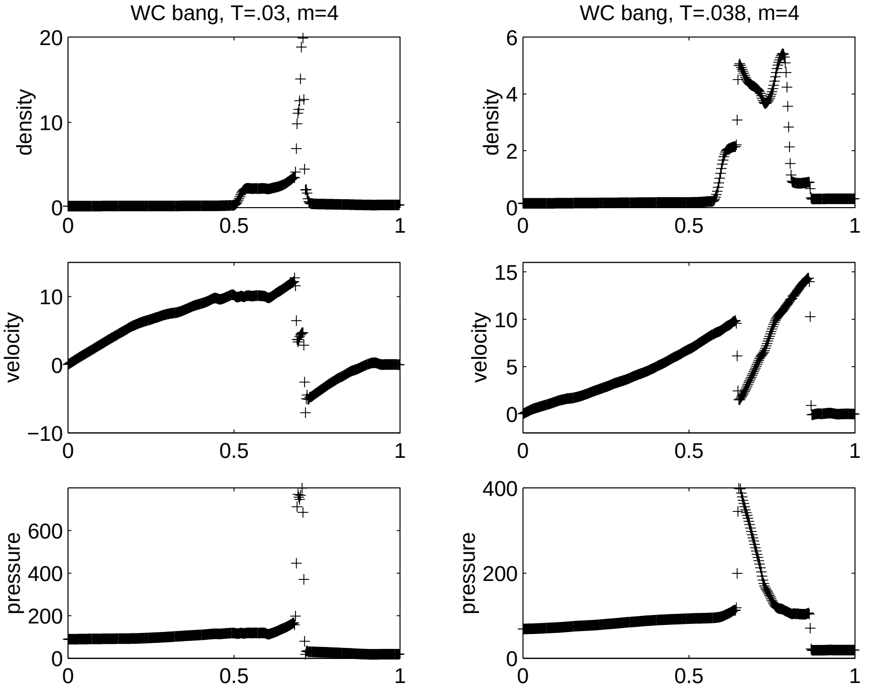

Fig. 4.8. *Solution of the Euler equations for Test* 6. $\lambda = 0.01$.

REFERENCES

[1] A. M. Anile, V. Romano, and G. Russo, *Hydrodynamical models for semiconductors based on extended thermodynamics*, VLSI Design, 8 (1998), pp. 521–525.

[2] F. Bianco, G. Puppo, and G. Russo, *Proceedings of the High Order Central Schemes for Hyperbolic Systems of Conservation Laws Conference*, HYP-98 Seventh International Conference on Hyperbolic Problems, Theory, Numerics, Applications, ETH Zürich, Switzerland, 1998.

[3] A. Harten, B. Engquist, S. Osher, and S. Chakravarthy, *Uniformly high order accurate essentially non-oscillatory schemes* III, J. Comput. Phys., 71 (1987), pp. 231–303.

[4] G. S. Jiang and E. Tadmor, *Non-Oscillatory Central Schemes for Multidimensional Hyperbolic Conservation Laws*, CAM Report 96-36, UCLA, Los Angeles, CA, 1996.

[5] P. D. Lax, *Weak solutions of non-linear hyperbolic equations and their numerical computation*, Comm. Pure Appl. Math., 7 (1954), pp. 159–193.

[6] R. J. LeVeque, *Numerical Methods for Conservation Laws*, Lectures in Mathematics, Birkhäuser-Verlag, Basel, Switzerland, 1992.

[7] D. Levy, G. Puppo, and G. Russo, *Central WENO Schemes for Hyperbolic Systems of Conservation Laws*, Ecole Normale Superieure report LMENS-98-17; Math. Model. Numer. Anal., to appear.

[8] D. Levy, G. Puppo, and G. Russo, *Central WENO Schemes for* 2*D Hyperbolic Systems of Conservation Laws*, in Proceedings of ICOSAHOM 98, D. Gottlieb, ed., Herzliya, Israel, 1998.

[9] D. Levy and E. Tadmor, *Non-oscillatory central differencing for the Incompressible* 2*-D Euler Equations*, CAM Report 96-37, UCLA, Los Angeles, CA, 1996.

[10] X. D. Liu and E. Tadmor, *Third order non-oscillatory central scheme for hyperbolic conservation laws*, Numer. Math., 79 (1998), pp. 397–425.

[11] H. Nessyahu and E. Tadmor, *Non-oscillatory central differencing for hyperbolic conservation laws*, J. Comput. Phys., 87 (1990), pp. 408–448.

[12] A. M. Rogerson and E. Meiburg, *A numerical study of the convergence properties of ENO schemes*, J. Sci. Comput., 5 (1990), pp. 151–167.

[13] V. Romano and G. Russo, *Numerical solution for hydrodynamical models of semiconductors*, Math. Models Methods Appl. Sci., submitted.

[14] R. Sanders and A. Weiser, *High Resolution Staggered Mesh Approach for Nonlinear Hyperbolic Systems of Conservation Laws*, J. Comput. Phys., 101 (1992), pp. 314–329.

[15] C. W. Shu, *Numerical experiments on the accuracy of ENO and modified ENO schemes*, J. Sci. Comput., 5 (1990), pp. 127–149.

[16] C. W. Shu and S. Osher, *Efficient Implementation of Essentially Non-Oscillatory Shock-Capturing Schemes*, II, J. Comput. Phys., 83 (1989), pp. 32–78.

[17] G. Sod, *A survey of several finite difference methods for systems of nonlinear hyperbolic conservation laws*, J. Comput. Phys., 22 (1978), pp. 1–31.

[18] P. Woodward and P. Colella, *The numerical simulation of two-dimensional fluid flow with strong shocks*, J. Comput. Phys., 54 (1984), pp. 115–173.

[19] M. Zennaro, *Natural Continuous Extensions of Runge-Kutta Methods*, Math. Comp. 46 (1986), pp. 119–133.